Cryogenic Transport Crossover and V-Shaped Subthreshold Swing Under EOT Scaling in Fully Depleted IGZTO TFTs

Kai Chen[1,2], Yunlong Li[1,2,3]*

[1]Zhejiang University, Hangzhou, China, [2]Zhejiang ICsprout Semiconductor Co., Ltd, Hangzhou, China
[3]State Key Laboratory of Silicon and Advanced Semiconductor Materials, Hangzhou, China *Email: bta@zju.edu.cn

***Abstract*—In this work, we experimentally investigate the impact of equivalent oxide thickness (EOT) scaling on the cryogenic transfer characteristics and carrier transport of fully depleted indium-gallium-zinc-tin-oxide (IGZTO) thin film transistors (TFTs) down to 4.8 K. Our measurements reveal a V-shaped subthreshold swing (SS) evolution upon cooling. Specifically, as the EOT decreases, the crossover temperature systematically shifts to higher values, while the minimum SS remains nearly unchanged. Transport analysis demonstrates that EOT scaling accelerates the crossover from extended-state transport to localized-state hopping, whereas the invariant low-temperature SS limit is mainly governed by the intrinsic band-tail states of the amorphous oxide channel. These results provide insight into cryogenic transport in amorphous oxide semiconductor (AOS) TFTs and guidance for cryogenic monolithic 3D integrated systems.**

***Keywords*—Cryogenic electrical characteristics, Subthreshold swing, Thin film transistors (TFTs), Equivalent oxide thickness scaling, Amorphous oxide, Variable-range hopping**

I. Introduction

Monolithic three-dimensional (M3D) integration [1]and cryogenic operation [2]are highly synergistic paradigms for next-generation energy-efficient computing. As illustrated in **Fig. 1**, while M3D maximizes integration density and minimizes interconnect overhead, cryogenic environments inherently suppress thermal noise and phonon scattering, significantly improving the subthreshold swing (SS) and transport efficiency of silicon CMOS logic [3, 4]. However, realizing the full potential of cryogenic M3D systems requires high-performance, back-end-of-line (BEOL) compatible memory and peripheral devices, which now represent the primary system bottleneck.

Amorphous oxide semiconductor (AOS) thin-film transistors (TFTs) have emerged as leading candidates for BEOL monolithic integration due to their low thermal budget and ultra-low off-state leakage [5, 6]. Nevertheless, unlike crystalline silicon, AOS materials possess a highly disordered electronic structure dominated by sub-gap band-tail states [7]. While cryogenic cooling conventionally steepens the SS toward the Boltzmann limit, the defect-mediated transport in AOS TFTs presents unique physical challenges at extremely low temperatures [8-11]. Specifically, how carrier conduction mechanisms and subthreshold characteristics evolve under both deep cryogenic conditions and aggressive equivalent oxide thickness (EOT) scaling remains fundamentally unexplored.

To address this critical gap, we investigate the cryogenic transfer characteristics of fully depleted IGZTO TFTs down to 4.8 K with EOT scaling. We unveil a pronounced, EOT-dependent V-shaped SS evolution, driven by a transport crossover from extended-state thermal activation to localized-state hopping. The crossover temperature is found to be strongly modulated by EOT scaling, while the minimum SS remains nearly constant, indicating that it is primarily determined by the intrinsic band-tail states of the AOS channel itself. These experimental findings reveal the physical limits of AOS TFTs at cryogenic temperatures and establish essential design guidelines for low-power cryogenic M3D architectures.

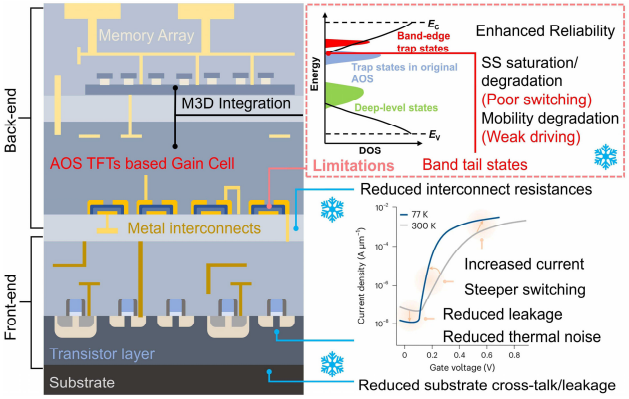

Fig. 1. Key technological advantages and the performance bottleneck of cryogenic M3D systems.

II. Device Fabrication and Measurement Details

A bottom-gate IGZTO TFT structure was employed in this work, as illustrated in **Fig. 2(a)**. A heavily doped p-type Si wafer served as the global gate. Al_2O_3 gate dielectrics with thicknesses of 10, 7, and 5 nm were then deposited via thermal atomic layer deposition at 250 °C. To ensure full channel depletion, an 5 nm IGZTO film was subsequently deposited by sputtering. Source/drain electrodes comprising 50 nm Ni were patterned via contact lithography, thermal evaporation, and a lift-off process. Finally, the active channel region was defined using wet etching.

Temperature-dependent electrical characterizations, ranging from 300 K down to 4.8 K, were performed in a Lake Shore cryogenic probe station. DC transfer characteristics were measured using a Keithley 4200A-SCS parameter analyzer equipped with remote preamplifiers. To suppress instrumentation and probe station noise at extreme low temperatures, SS was extracted from the linear region of the log I_D-V_{GS} curves within a specific current window (10^{-8}-10^{-7} μA/μm). The threshold voltage (V_{th}) was defined via the constant-current method at I_D = 100 nA×W/L, where W and L are the channel width and length, respectively. The field-effect mobility (μ_{FE}) was extracted from the

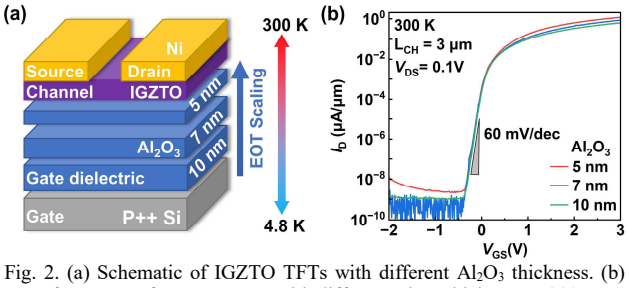

Fig. 2. (a) Schematic of IGZTO TFTs with different Al_2O_3 thickness. (b) Transfer curves of IGZTO TFTs with different Al_2O_3 thickness at 300 K.

transconductance of the transfer curves.

III. Results and Discussion

The transfer characteristics at 300 K for IGZTO TFTs with Al_2O_3 thicknesses of 10, 7, and 5 nm are shown in **Fig. 2(b)**. Notably, in the subthreshold region, the three curves nearly overlap across all dielectric thicknesses. This uniformity originates from the fully depleted 5 nm IGZTO channel, in which the channel potential is strongly controlled by the gate before substantial carrier accumulation occurs. It also confirms that dielectric scaling does not introduce parasitic doping effects. Accordingly, the extracted SS remains close to the thermal limit at 300 K (~60 mV/dec), indicating excellent electrostatic control and a low interfacial trap density. As V_{GS} further increases, the drain current becomes larger for thinner Al_2O_3, consistent with the higher gate-oxide capacitance and stronger electrostatic coupling associated with smaller EOT.

A. Cryogenic Transfer Characteristics and SS Evolution

Fig. 3(a)–(c) show the transfer curves of fully depleted IGZTO TFTs with Al_2O_3 thicknesses of 10, 7, and 5 nm, measured from 300 K down to 4.8 K. For all devices, the transfer curves shift positively as the temperature decreases, consistent with previous observations in AOS TFTs [7, 10, 11]. The extracted V_{th} is summarized in **Fig. 3(d)**, where a monotonic increase is observed with decreasing temperature. This behavior is mainly attributed to the increase in Fermi potential and bandgap widening at low temperatures [12]. Compared with the thicker dielectric devices, EOT scaling slightly suppresses the magnitude of the V_{th} shift. Nevertheless, no clear saturation of V_{th} is observed down to 4.8 K, suggesting that cryogenic cooling alone does not reduce the required operating voltage in IGZTO TFTs.

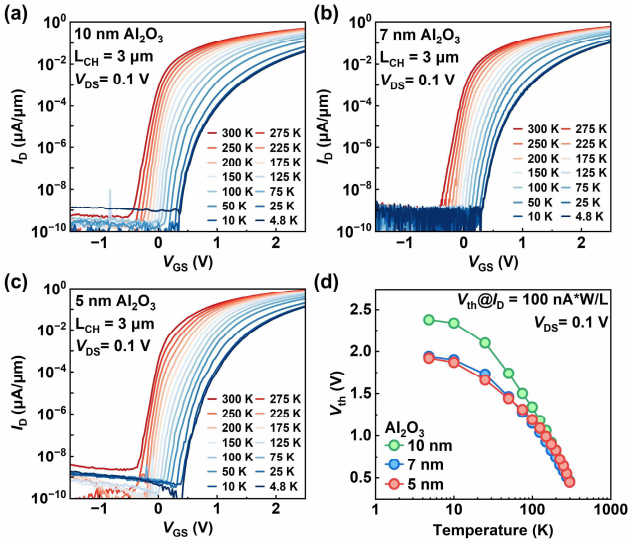

Fig. 3. (a)–(c) Transfer curves of IGZTO TFTs with 10 nm, 7 nm and 5 nm Al_2O_3, respectively, measured from 300 K down to 4.8 K, respectively. (d) Extracted V_{th} versus temperature with different Al_2O_3 thicknesses.

The temperature-dependent SS extracted from 300 K to 4.8 K is shown in **Fig. 4(a)–(c)** for devices with different Al_2O_3 thicknesses. To ensure statistical reliability, the SS at each temperature was extracted from 3–4 devices with the same configuration. At first, the SS decreases nearly linearly with decreasing temperature for all EOTs. Moreover, reducing the Al_2O_3 thickness drives the SS closer to the thermal prediction SS = $\ln 10 k_B T/q$ [13], where k_B is the Boltzmann constant, T is the absolute temperature, and q is

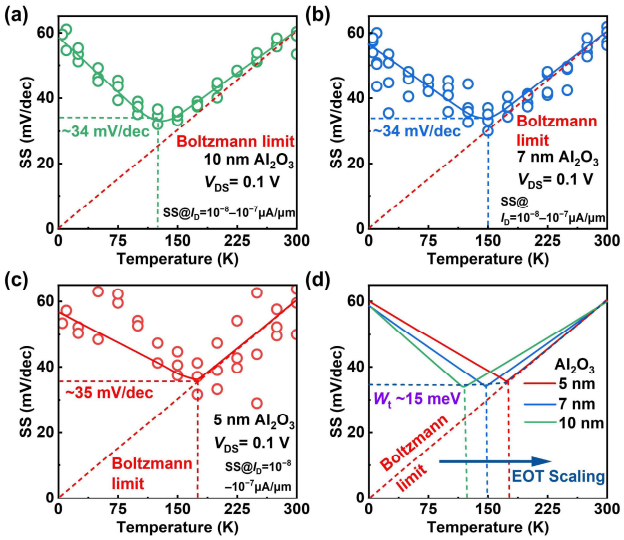

Fig. 4. (a)–(c) Temperature-dependent SS for IGZTO TFTs with different Al_2O_3 thickness. (d) Summary plot of SS as a function of temperature for devices with different Al_2O_3 thicknesses.

the electron charge. This trend reflects the stronger gate control enabled by smaller EOT. As the temperature is further reduced, however, the SS no longer follows the thermal trend. Instead, each device reaches a minimum value of ~34–35 mV/dec before increasing at lower temperatures, eventually returning to ~60 mV/dec near 4.8 K. The summary plot in **Fig. 4(d)** reveals a pronounced V-shaped SS evolution. Importantly, the crossover temperature (T_c), corresponding to the minimum SS, shifts systematically to higher values with decreasing Al_2O_3 thickness: ~125 K for 10 nm, ~150 K for 7 nm, and ~175 K for 5 nm. In contrast, the minimum SS itself remains nearly unchanged for all three EOTs, staying close to ~34–35 mV/dec.

This saturation behavior is well captured by a band-tail model—previously adopted to explain cryogenic SS saturation in silicon transistors [4]—where potential-fluctuation-induced tail states impose a lower bound: $SS_{sat} = \ln 10 W_t/q$. Here, W_t represents the characteristic width of the band-tail states. Because the channel thickness, composition, and fabrication process are identical for all devices, this intrinsic disorder remains essentially unchanged, yielding a narrowly distributed minimum SS of ~34–35 mV/dec across all EOT splits. Using the minimum SS as an effective band-tail indicator, an effective tail parameter of ~15 meV is obtained. This value is comparable to previously reported cryogenic values in oxide TFTs, such as ~17 meV in 10 nm IGZO [10] and ~13 meV in 4 nm ITO [11], suggesting that Sn incorporation in IGZTO may help maintain a relatively smooth electron transport landscape while preserving the amorphous nature of the channel. More importantly, unlike the classical monotonic saturation picture often invoked for silicon transistors, the present IGZTO TFTs exhibit a clear V-shaped SS evolution: the SS first approaches an effective tail-related minimum and then rises again at deeper cryogenic. This behavior implies that an additional low-temperature transport crossover occurs below T_c.

B. Cryogenic Transport Crossover Under EOT Scaling

To elucidate the physical origin of the V-shaped SS reversal, the temperature-dependent conduction mechanisms were analyzed. In the high temperature regime, the transfer characteristics are evaluated using the Arrhenius relationship: $\ln(I_D/T^{1.5}) \propto -E_a/k_B T$ [14], where E_a is the

activation energy. As shown in **Fig. 5(a)–(c)**, the Arrhenius plots exhibit highly linear fits across all applied gate biases within their respective temperature windows: 300–125 K for 10 nm Al_2O_3, 300–150 K for 7 nm, and 300–175 K for 5 nm. This linearity indicates that transport is dominated by thermally activated carriers excited above the mobility edge (E_m). From these Arrhenius slopes, the effective channel barrier height (Φ_B=E_a) was extracted as a function of V_{GS}, as summarized in **Fig. 5(d)**. For all dielectric thicknesses, Φ_B decreases with increasing V_{GS}, and this dependence becomes steeper for thinner Al_2O_3. To decouple channel and contact effects, the contact Schottky barrier height (Φ_{SB}) was estimated from the flat-band condition, identified as the gate bias where Φ_B no longer follows its initial linear dependence on V_{GS}. The extracted Φ_{SB} is approximately ~31 meV and remains nearly invariant across all three dielectric thicknesses. This consistency indicates that EOT scaling does not materially modify the injection barrier in the temperature range above the crossover point. Therefore, the observed EOT-dependent cryogenic trends originate intrinsically from gate control over the channel rather than

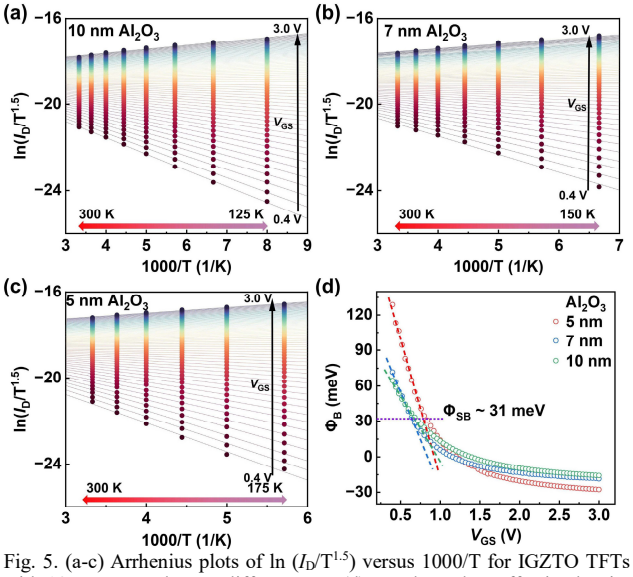

Fig. 5. (a-c) Arrhenius plots of ln (I_D/$T^{1.5}$) versus 1000/T for IGZTO TFTs with 10, 7, 5 nm Al_2O_3 at different V_{GS}. (d) V_{GS}-dependent effective barrier height (ΦB) for IGZTO TFTs with 10, 7, and 5 nm Al_2O_3.

from contact-limited transport.

Below the crossover temperature, the thermal energy becomes insufficient to excite carriers above E_m, forcing them to freeze into the sub-gap localized states. The data were therefore analyzed using the three-dimensional Mott variable-range hopping (VRH) [15], described by $\ln(I_D) \propto -(T_0/T)^{1/4}$ [16], where T_0 is the characteristic temperature related to the density of localized states and the localization length. As shown in **Fig. 6(a)–(c)**, lnI_D varies linearly with $T^{-1/4}$ in an intermediate low-temperature range, confirming VRH-type hopping conduction after the first crossover. Specifically, the VRH regime extends from 125 K to 50 K for the 10 nm device, and from 150 K to 75 K and 175 K to 75 K for the 7 nm and 5 nm devices, respectively. At deeper cryogenic temperatures, however, the simple Mott-VRH model can no longer describe the measured current. This second deviation suggests that another limiting process becomes relevant below a second characteristic temperature (T_{C2}), possibly involving carrier freeze-out, depletion of

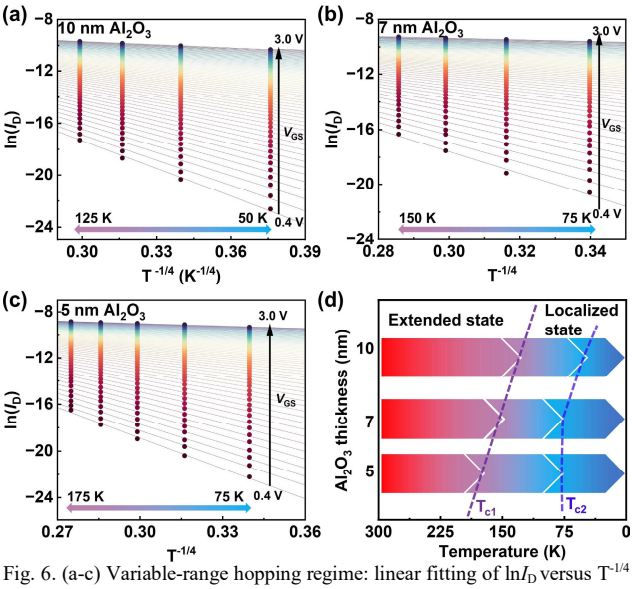

Fig. 6. (a-c) Variable-range hopping regime: linear fitting of lnI_D versus $T^{-1/4}$ for IGZTO TFTs with 10, 7, 5 nm Al_2O_3 at different V_{GS}. (d) Transport regime map summarizing the evolution of carrier transport mechanisms in IGZTO as a function of Al_2O_3 thickness and temperature.

accessible hopping paths, tunneling-assisted hopping, or a growing contribution from contact-limited injection [2]. The transport regime map in **Fig. 6(d)** therefore identifies two characteristic temperatures: T_{C1}, corresponding to the crossover from thermally activated extended-state transport to localized-state hopping, and T_{C2}, marking the lower-temperature boundary where transport departs from the simple VRH picture. Importantly, both T_{C1} and T_{C2} shift to higher temperatures as the Al_2O_3 thickness decreases, showing that EOT scaling systematically accelerates the

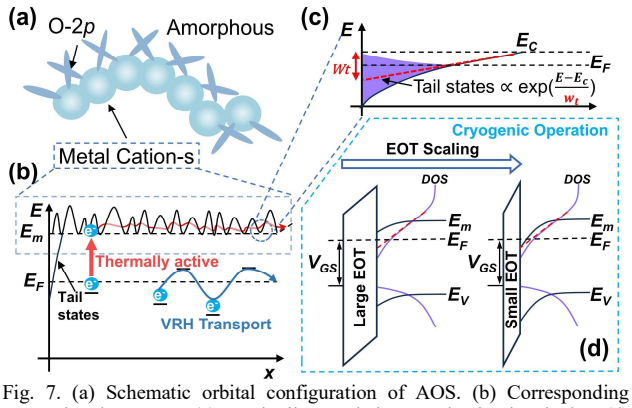

Fig. 7. (a) Schematic orbital configuration of AOS. (b) Corresponding energy band structure. (c) Band tail states below conduction band edge. (d) Low-temperature energy-band evolution under the same gate bias.

transport crossover.

This behavior can be understood from the electronic structure of AOS, as illustrated in **Fig. 7**. In AOS materials, the conduction-band edge is mainly formed by spatially extended metal-cation s orbitals [6], as schematically shown in **Fig. 7(a)** and **(b)**. Because these orbitals are nearly isotropic and relatively insensitive to local bond-angle disorder, they can sustain efficient electron transport at sufficiently high temperatures through states above the mobility edge. However, structural disorder and interface-related perturbations inevitably generate localized band-tail states below the conduction-band edge, as shown in **Fig. 7(c)**. As the temperature decreases, thermal activation toward the extended states becomes less effective, and

transport gradually changes to hopping through localized tail states near the Fermi level [7, 17]. At still lower temperatures, the accessible hopping network becomes increasingly restricted, leading to deviation from simple Mott-VRH behavior. Under the same V_{GS}, a smaller EOT produces stronger electrostatic coupling and a larger effective electric field in the channel, as illustrated in **Fig. 7(d)**, thereby accelerating the crossover from extended-state transport to localized-state transport. This EOT-dependent transport crossover directly correlates with the EOT-dependent temperature shift of the SS minimum.

C. Mobility Evolution at Cryogenic Temperatures

Besides subthreshold characteristics, the temperature-dependent mobility is another crucial metric for evaluating the performance of cryogenic M3D systems. **Fig. 8(a)** shows the μ_{FE}–V_{GS} characteristics of the IGZTO TFT with 5 nm Al_2O_3 from 300 K to 4.8 K. As the temperature decreases, the curves shift toward higher V_{GS}. Meanwhile, μ_{FE} shows a slight increase at first, followed by a gradual decrease, with a pronounced drop below ~175 K. **Fig. 8(b)** compiles the temperature-dependent μ_{FE} extracted at V_{GS} = 2.5 V for all Al_2O_3 thicknesses. Smaller EOTs consistently yield higher mobility. In addition, for all devices, μ_{FE} shows only a small variation down to a specific critical temperature, followed by a rapid decrease at deeper cryogenic temperatures. This onset of mobility degradation generally aligns with the respective crossover temperature T_{C1}, consistent with the transition from extended-state transport to localized-state hopping.

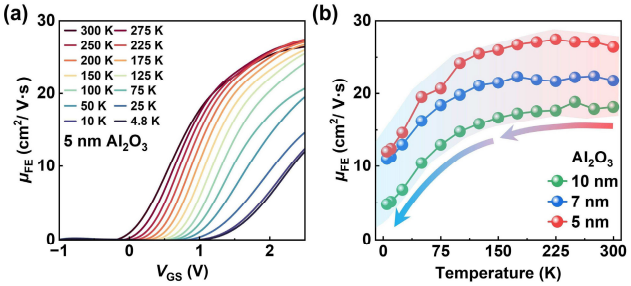

Fig. 8. (a) Field-effect mobility μ_{FE} versus V_{GS} for the IGZTO TFT with 5 nm Al_2O_3 from 300 K to 4.8 K. (b) μ_{FE} at V_{GS} = 2.5 V as a function of temperature for IGZTO TFTs with different Al_2O_3 thickness.

Finally, **Fig. 9** compares the temperature-dependent SS of different transistor technologies. Bulk-Si [4] and FD-SOI [3] FETs follow the Boltzmann limit over a wide cryogenic range and then saturate at ~20 K due to band-tail effects. In contrast, AOS TFTs show a more diverse low-temperature behavior, including saturation or deep-cryogenic upturn. Compared with reported IGZO TFTs [10], the IGZTO TFTs in this work exhibit a weaker low-temperature SS upturn and remain closer to the thermal limit, while ITO TFTs [11] show an even more gradual evolution. These comparisons suggest that cation engineering and improved structural order

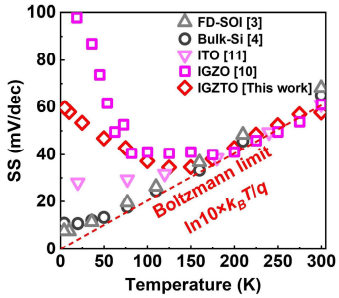

Fig. 9. Comparison of SS with temperature for FD-SOI, bulk-Si FETs and AOS TFTs.

are effective routes to suppress cryogenic SS degradation in AOS TFTs[18].

IV. Conclusion

In summary, fully depleted IGZTO TFTs under EOT scaling were experimentally investigated from 300 K down to 4.8 K. All devices maintained near-ideal SS of ~60 mV/dec at 300 K, while showing an EOT-dependent V-shaped SS evolution at cryogenic temperatures. The crossover temperature shifted to higher values as EOT decreased, reflecting an accelerated transition from extended-state transport to localized-state hopping, followed by an additional deep-cryogenic deviation from simple VRH behavior. These results show that EOT scaling mainly modulates the onset of transport crossover, whereas the low-temperature SS limit is governed primarily by the intrinsic band-tail states of the IGZTO channel.

Acknowledgment

This work was supported by the Hangzhou West Science and Technology Innovation Fund (No. 134000-X02402/006).

References

[1] M. M. S. Aly et al., "The N3XT approach to energy-efficient abundant-data computing," Proc. IEEE, vol. 107, no. 1, pp. 19-48, 2018.

[2] C. Zota et al., "Energy-efficient computing at cryogenic temperatures," Nature Electronics, vol. 7, no. 11, pp. 966-974, 2024.

[3] H. Bohuslavskyi et al., "Cryogenic subthreshold swing saturation in FD-SOI MOSFETs described with band broadening," EDL, vol. 40, no. 5, pp. 784-787, 2019.

[4] A. Beckers et al., "Theoretical limit of low temperature subthreshold swing in field-effect transistors," EDL, vol. 41, no. 2, pp. 276-279, 2019.

[5] A. Belmonte and G. S. Kar, "Disrupting the DRAM roadmap with capacitor-less IGZO-DRAM technology," Nature Reviews Electrical Engineering, vol. 2, pp. 220–221, 2025.

[6] K. Nomura et al., "Room-temperature fabrication of transparent flexible thin-film transistors using amorphous oxide semiconductors," Nature, vol. 432, no. 7016, pp. 488-492, 2004.

[7] S. Lee and A. Nathan, "Localized tail state distribution in amorphous oxide transistors deduced from low temperature measurements," APL, vol. 101, no. 11, p. 113502, 2012.

[8] S. Lee et al., "Trap-limited and percolation conduction mechanisms in amorphous oxide semiconductor thin film transistors," APL, vol. 98, no. 20, p. 203508, 2011.

[9] S. Lee et al., "Temperature dependent electron transport in amorphous oxide semiconductor thin film transistors," IEDM, 2011, pp. 14.6. 1-14.6. 4.

[10] H. Tang et al., "Subthreshold swing behavior in amorphous indium-gallium-zinc-oxide transistors from room to cryogenic temperatures," APL, vol. 126, no. 23, p. 232108, 2025.

[11] J. Kang et al., "Investigation of Physical Limits of Low Temperature Subthreshold Swing in Indium-Tin-Oxide Transistors," EDL, vol. 46, no. 6, pp. 995-998, 2025.

[12] A. Beckers et al., "Physical model of low-temperature to cryogenic threshold voltage in MOSFETs," JEDS, vol. 8, pp. 780-788, 2020.

[13] E. A. Gutierrez-D et al., Low temperature electronics: physics, devices, circuits, and applications. Academic Press, 2001.

[14] C. Niu et al., "Surface Accumulation Induced Negative Schottky Barrier and Ultralow Contact Resistance in Atomic-Layer-Deposited In 2 O 3 Thin-Film Transistors," TED, vol. 71, no. 5, pp. 3403-3410, 2024.

[15] W. Chakraborty et al., "Low thermal budget (< 250° C) dual-gate amorphous indium tungsten oxide (IWO) thin-film transistor for monolithic 3-D integration," TED, vol. 67, no. 12, pp. 5336-5342, 2020.

[16] N. Mott, "The effect of electron interaction on variable-range hopping," The Philosophical Magazine, vol. 34, no. 4, pp. 643-645, 1976.

[17] J. Guo et al., "Analytical surface potential-based compact model for independent dual gate a-IGZO TFT," TED, vol. 68, no. 4, pp. 2049-2055, 2021.

[18] H. Jang et al., "InGaZnO4 and In2O3 Mobility Trend: The Role of Structural Disorder from Amorphous to Crystalline States," ACS Materials Letters, vol. 7, no. 6, pp. 2024-2030, 2025.